CHAPTER IV
NON-ISOTHERMAL MELT-CRYSTALLIZATION KINETICS OF POLY(TRIMETHYLENE TEREPHTHALATE)

ABSTRACT

Non-isothermal melt-crystallization kinetics and subsequent melting behavior of poly(trimethylene terephthalate) (PTT) have been investigated by differential scanning calorimetry (DSC) technique. The Avrami, Tobin and Ozawa equations were applied to describe the kinetics of the crystallization process. Both of the Avrami and Tobin crystallization rate parameters (i.e. K_A and K_T, respectively) were found to increase with increasing cooling rate. The Ozawa crystallization rate K_O was found to decrease with increasing temperature. The ability of PTT to crystallize from the melt under a unit cooling rate was determined by the Ziabicki's kinetic crystallizability index G_Z, which was found to be ca. 0.98. The effective energy barrier describing the non-isothermal melt-crystallization process ΔE of PTT was estimated by the differential iso-conversional method of Friedman and was found to increase with an increase in the relative crystallinity. In its subsequent melting, PTT exhibited triple endothermic melting behavior when it was cooled at cooling rates lower than ca. $20^{\circ}C \cdot min^{-1}$, while it exhibited double endothermic melting behavior when it was cooled at cooling rates greater than ca. $20^{\circ}C \cdot min^{-1}$.

(**Key-words:** poly(trimethylene terephthalate); non-isothermal melt-crystallization behavior; subsequent melting behavior)

1. INTRODUCTION

Poly(trimethylene terephthalate) (PTT) is a linear aromatic polyester which was first synthesized by Whinfield and Dickson in 1941 [1]. At that time, it was not available commercially because of the high production cost of one of the main reactants, 1,3-propanediol (PDO). However, recent breakthroughs in PDO synthesis via hydroformylation of ethylene oxide, process improvements in traditional synthetic route through acrolein, and promising bioengineering route have reduced the cost of it [2]. This led to the production of PTT for commercial uses, joining other well-known linear aromatic polyesters, such as poly(ethylene terephthalate) (PET) and poly(buthylene terephthalate) (PBT). Prospective uses for PTT are in areas such as fibers, films, and engineering thermoplastics. Mechanical properties of PTT lie roughly between those of PET and PBT. Of interest is that PTT showed a better tensile elastic recovery and a lower modulus than PET and PBT [3].

Since both physical and mechanical properties of a semi-crystalline polymer are strongly dependent on the extent of crystallization and morphology developed during processing, studies related to crystallization kinetics are key information to gain an understanding on the relationship among the processing conditions, the structure developed, and the properties observed in a final polymeric product.

Studies related to the chain conformation, crystal structure, and morphology of PTT have been carried out and reported in recent years [4-6]. A few studies related to the subject of isothermal melt-crystallization kinetics of PTT include Avrami crystallization kinetics [7-11] and the kinetics of the linear spherulitic growth rates [8,9,12]. We have earlier reported some information about non-isothermal melt-crystallization kinetics of PTT in comparison with PET and PBT [13] and non-isothermal melt-crystallization kinetics of PTT and its blends with PBT [14].

Despite the similarity with our two earlier reports [13-14], the present contribution is aimed at studying the non-isothermal melt-crystallization kinetics of PTT in full detail. The experimental data were also collected in a narrower cooling rate range of 5 to 30°C·min^{-1}, with a much smaller increment between adjacent cooling rates. The experimental data obtained from the differential scanning calorimetry (DSC) technique were thoroughly analyzed based on the Avrami, Tobin, Ozawa, and Ziabicki macrokinetic models. The effective energy barrier describing

the non-isothermal melt-crystallization process of PTT was estimated based on the differential iso-conversional method of Friedman.

2. THEORITICAL BACKGROUND

In the study of non-isothermal crystallization using DSC, the energy released during the crystallization process appears to be a function of temperature rather than time as in the case of isothermal crystallization. As a result, the relative crystallinity function of temperature $\theta(T)$ can be formulated as

$$\theta(T) = \frac{\int_{T_0}^{T} \left(\frac{dH_c}{dT} \right) dT}{\Delta H_c}, \tag{1}$$

where T_0 and T represent the onset and an arbitrary temperature, respectively, dH_c is the enthalpy of crystallization released during an infinitesimal temperature range dT, and ΔH_c is the total enthalpy of crystallization for a specific cooling condition.

To use Equation (1) to analyze non-isothermal crystallization data obtained by DSC, it is assumed that the sample experiences the same thermal history as designated by the DSC furnace. This may be realized only when the lag between the temperatures of the sample and the furnace is kept minimal. If this assumption is valid, the relation between the crystallization time t and the sample temperature T can be formulated as

$$t = \frac{T_0 - T}{\phi}, \tag{2}$$

where T_0 is an arbitrary reference melt temperature and ϕ is the cooling rate. According to Equation (2), the horizontal temperature axis observed in a DSC thermogram for the non-isothermal crystallization data can be transformed into the time scale.

The most common approach to describe the overall isothermal crystallization kinetics is the Avrami model [15-17], in which the relative crystallinity function of time $\theta(t)$ can be expressed in the following form:

$$\theta(t) = 1 - \exp[-(K_A t)^{n_A}] \in [0,1], \tag{3}$$

where K_A and n_A are the Avrami crystallization rate constant and the Avrami exponent, respectively. Both K_A and n_A are constants specific to a given crystalline morphology and type of nucleation for a particular crystallization condition [18] and, based on the original assumptions of the theory, the value of n_A should be an integer ranging from 1 to 4. It should be noted that the units of K_A are given as an inverse of time. Although, the Avrami equation is often used to describe the isothermal crystallization behavior of a semi-crystalline polymer, it has also been applied to describe the non-isothermal crystallization behavior of a semi-crystalline polymer [13,19,20].

A major drawback of the Avrami approach is that the model is only suitable for describing the early stages of crystallization. Complications arise from the effects of growth site impingement and secondary crystallization process, which were disregarded for the sake of simplicity in the original derivation of the model. A theory for phase transformation kinetics with growth site impingement was proposed by Tobin [21-23]. According to this approach, the relative crystallinity function of time $\theta(t)$ can be expressed in the following form:

$$\theta(t) = \frac{(K_T t)^{n_T}}{1 + (K_T t)^{n_T}} \in [0,1], \tag{4}$$

where K_T and n_T are the Tobin crystallization rate constant and the Tobin exponent, respectively. Based on this proposition, n_T needs not be an integer [21-23] and is also governed by different types of nucleation and growth mechanisms. It should be noted that the units of K_T are given as an inverse of time.

Based on the mathematical derivation of Evans [24], Ozawa extended the Avrami theory to be able to describe the non-isothermal crystallization case by assuming that the sample was cooled (or heated) with a constant rate from the molten state (or the amorphous state) [25]. In the Ozawa method, the time variable in the Avrami equation was replaced by a cooling (or heating) rate and the relative crystallinity was derived as function of constant cooling (or heating) rate ϕ as

$$\theta(T) = 1 - \exp\left[-\left(\frac{K_O}{\phi}\right)^{n_O}\right], \tag{5}$$

where K_O and n_O are the Ozawa crystallization rate constant and the Ozawa exponent, respectively. Both of the Ozawa kinetic parameters (i.e. K_O and n_O) hold a similar physical meaning to those of the Avrami ones (i.e. K_A and n_A). Analytically, the Ozawa kinetic parameters (i.e. K_O and n_O) can be extracted from a least-squared line drawn through the bulk of the data according to the double-logarithmic plot of $\ln[-\ln(1-\theta(T))]$ versus $\ln(\phi)$ for a fixed temperature, in which K_O and n_O can be determined from the y-intercept and the slope, respectively.

Instead of describing the crystallization process with complicated mathematical models, Ziabicki [26-28] proposed that the kinetics of polymeric phase transformation can be described by a first-order kinetic equation of the form:

$$\frac{d\theta(t)}{dt} = K_Z(T)[1-\theta(t)], \tag{6}$$

where $K_Z(T)$ is a temperature-dependent crystallization rate function. In case of non-isothermal crystallization, both $\theta(t)$ and $K_Z(T)$ vary and are dependent on the cooling rate used. For a given cooling condition, Ziabicki [26-28] showed that the crystallization rate function $K_Z(T)$ can be described by a Gaussian function of the following form:

$$K_Z(T) = K_{Z,max} \exp\left[-4\ln 2\frac{(T-T_{max})^2}{D^2}\right], \tag{7}$$

where T_{max} is the temperature at which the crystallization rate is maximum, $K_{Z,max}$ is the crystallization rate at T_{max}, and D is the width at half-height determined from the crystallization rate function. With use of the isokinetic approximation, integration of Equation (7) over the whole crystallizable range (i.e. $T_g < T < T_m^0$) leads to an important characteristic value describing the crystallization ability of a semi-crystalline polymer, i.e. the kinetic crystallizability index G_Z:

$$G_Z = \int_{T_g}^{T_m^0} K_Z(T)dT \approx 1.064 K_{Z\,max} D. \tag{8}$$

According to the approximate theory [26], the parameter G_Z describes the ability of a semi-crystalline polymer to crystallize when it is cooled at unit cooling rate [28].

In case of non-isothermal crystallization studies using DSC, Equation (8) can be applied when the crystallization rate function $K_Z(T)$ is replaced with a

derivation function of the relative crystallinity $(d\theta/dT)_\phi$ specific for each cooling rate studied (i.e. crystallization rate function at different cooling rates). Therefore, Equation (8) is replaced by

$$G_{Z,\phi} = \int_{T_g}^{T_m^0} (d\theta/dT)_\phi \, dT \approx 1.064 (d\theta/dT)_{\phi,max} D_\phi , \quad (9)$$

where $(d\theta/dT)_{\phi,max}$ and D_ϕ are the maximum crystallization rate and the width at half-height of the $(d\theta/dT)_\phi$ function. According to Equation (9), $G_{Z,\phi}$ is the kinetic crystallizability index for an arbitrary cooling rate ϕ. The Ziabicki kinetic crystallizability index G_Z can therefore be obtained by normalizing $G_{Z,\phi}$ with ϕ (i.e. $G_Z = G_{Z,\phi}/\phi$). This procedure was first realized by Jeziorny [29].

While offering a simple way for evaluating corresponding kinetic parameters specific to each model, the Avrami, Tobin, and Ozawa analyses do not suggest a means for evaluating the effective energy barrier for non-isothermal crystallization process ΔE. In light of this, various mathematical procedures [30-32] had been proposed for evaluating the ΔE value. The main objective of these methods is to define a finite relationship between the peak temperature T_p obtained for a given condensed phase transformation reaction and the heating rate ϕ used. A major concern for use of these procedures in obtaining the kinetic information for non-isothermal crystallization process which occurs on cooling has been raised [33], since the original mathematical expression of these procedures does not permit substitution of negative heating rates (i.e. cooling rates). However, this problem has largely been mistakenly avoided by dropping off the minus sign in the negative heating rates (see, for examples, ref. [19]).

For a process that occurs on cooling such as non-isothermal crystallization of polymer melts, reliable values of the effective energy barrier can be obtained, for examples, by the differential iso-conversional method of Friedman [34] or by the integral iso-conversional method of Vyazovkin [35-36]. In this work, the Friedman method will be used, due mainly to the reliability and simplicity of the method [33,36]. The Friedman equation is expressed as

$$\ln\left(\dot{\theta}_\theta(t)\right) = A - \frac{\Delta E_\theta}{RT}, \quad (10)$$

where $\dot{\theta}_\theta(t)$ is the instantaneous crystallization rate function of time at a given relative crystallinity θ, A is an arbitrary pre-exponential parameter, and ΔE_θ is the effective energy barrier of the process for a given relative crystallinity θ. By plotting the $\dot{\theta}_\theta(t)$ function obtained at various cooling rates against the corresponding inversed temperature for a given θ, the effective energy barrier for non-isothermal crystallization process can finally be determined.

3. EXPERIMENTAL DETAILS

3.1. Materials

The PTT sample used in this study was supplied in pellet form by Shell Chemicals Company (USA) (Corterra CP509201). The weight- and number-average molecular weights of this resin were kindly determined by Dr. Hoe Chuah and his colleagues of Shell Chemicals Company (USA) based on size-exclusion chromatography (SEC), to be ca. 78,100 and 34,700 Daltons, respectively.

3.2. Sample preparation and experimental procedure

PTT pallets were dried in a vacuum oven at 140°C for 5 hours prior to further use. Films of approximately 200 μm in thickness were obtained by melt-pressing dried pellets at 260°C in a Wabash V50H compression press under an applied hydraulic force of 10 tons. After 5 min holding time, the films were cooled down, while being in the compression press, to room temperature. The cooling of the platens of the compression press was by running cold water through channels in the platens and the cooling rate of the platens could be approximated by an exponential temperature-time decay, with a time constant of ca. 3 min.

A Perkin-Elmer Series 7 DSC (DSC-7) was used to study non-isothermal melt-crystallization kinetics of PTT. Temperature calibration was carried out using an indium standard (T_m^0 = 156.6°C and ΔH_f^0 = 28.5 J g^{-1}). The consistency of the temperature calibration was checked every other run to ensure the reliability of the data obtained. To minimize thermal lag between the polymer sample and the DSC furnace, each sample holder was loaded with a disc-shaped specimen, weighing

around 8.0 ± 0.5 mg, which was cut from the as-prepared films. Each sample was used only once and all the runs were preformed under nitrogen atmosphere to minimize thermal degradation.

The non-isothermal crystallization experiment started with heating each sample from 30°C at a heating rate of 80°C·min^{-1} to 275°C, where it was held for 5 min to ensure complete melting [37]. This thermal treatment was aimed at resetting the thermal history of all the samples investigated. After complete melting, each sample was cooled down at a specified cooling rate ϕ, ranging from 5 to 30°C·min^{-1}, to 25°C. The non-isothermal melt-crystallization exotherms were recorded for further analysis according to the aforementioned macrokinetic models. The subsequent melting behavior of each sample was recorded immediately after each cooling scan at a heating rate of 10°C·min^{-1}.

4. RESULTS AND DISCUSSION

4.1. Non-isothermal melt-crystallization and subsequent melting behavior

The non-isothermal melt-crystallization exotherms of PTT recorded at eight different cooling rates ranging from 5 to 30°C·min^{-1} are presented in Figure 1. Obviously, the crystallization exotherm becomes wider and shifts to a lower temperature with increasing cooling rate, as would be expected for crystallization in a nucleation-controlled region. In order to obtain the kinetic information, the experimental data such as those shown in Figure 1 need to be converted to the relative crystallinity function of temperature $\theta(T)$ using Equation (1). The converted $\theta(T)$ curves are shown in Figure 2. Based on these curves, some kinetic data [e.g. the temperature at 1% relative crystallinity $T_{0.01}$, the temperature at the maximum crystallization rate (i.e. peak temperature) T_p, and the temperature at 99% relative crystallinity $T_{0.99}$] can be taken and the values of these parameters are summarized in Table 1. Apparently, the $T_{0.01}$, T_p, and $T_{0.99}$ values are all shifted towards lower temperatures when the cooling rate increases. It should be noted that both $T_{0.01}$ and $T_{0.99}$ values represent the apparent onset and ending temperatures of the non-isothermal melt-crystallization process.

The data can be further analyzed by converting the temperature scale of the $\theta(T)$ function into the time scale, using Equation (2), to obtain the relative crystallinity function of time $\theta(t)$. The converted curves (shown as various geometrical points) are illustrated in Figure 3. According to Figure 3, It is clear that the faster the cooling rate, the shorter the time required for the completion of the crystallization process. It is important to note that all of the $\theta(t)$ curves shown do not include the apparent incubation period Δt_{inc}, which can be defined as a time period (viz. $\Delta t_{inc} = (T_f - T_{onset})/\phi$, where T_f is the fusion temperature or the temperature where a polymer sample is brought to melt, T_{onset} is the actual temperature where the sample begins to crystallize, and ϕ is the cooling rate), during which the polymer is still in its molten state. The Δt_{inc} values have been calculated based on the T_f value of 275°C [37] and are summarized in Table 2. Obviously, the Δt_{inc} parameter is found to monotonically decrease from ca. 15.8 min at $5^{\circ}C \cdot min^{-1}$ to ca. 3.1 min at $30^{\circ}C \cdot min^{-1}$.

In order to quantify the bulk kinetics of the non-isothermal melt-crystallization process, the crystallization time at an arbitrary relative crystallinity (i.e. t_θ) can be determined from the $\theta(t)$ functions shown in Figure 3. The t_θ values (after exclusion of the apparent incubation period Δt_{inc}) for various relative crystallinities θ (i.e. at the θ values of 0.01, 0.1, 0.3, 0.5, 0.7, 0.9, and 0.99, respectively) are summarized in Table 2 and are plotted as a function of cooling rate in Figure 4. The $t_{0.01}$ and $t_{0.99}$ values are qualitative measures of the beginning and the ending of the crystallization process. From the $t_{0.01}$ and $t_{0.99}$ values, the apparent total crystallization period Δt_c can be calculated (i.e. $\Delta t_c = t_{0.99} - t_{0.01}$) and the results are summarized in Table 2. Clearly, the way in which the t_θ value for a fixed θ value and the Δt_c value are all found to decrease with increasing cooling rate suggests that non-isothermal melt-crystallization proceeds faster with an increase in the cooling rate. In an attempt to further analyze the results obtained, plots of $\ln(\Delta t_c)$ against $\ln(\phi)$ (shown as the inset figure in Figure 4) and of $\ln(t_\theta)$ against $\ln(\phi)$ (shown as Figure 5) were carried out. Apparently, a linear relationship is observed on these

plots and, interestingly, all of the plots exhibit a similar slope (see Table 3), with the average value being ca. –0.725 $min^{2}\cdot{}^{o}C^{-1}$.

The subsequent melting thermograms for PTT (recorded with a heating rate 10°C min^{-1}) after non-isothermal melt-crystallization in DSC at eight different cooling rates were shown in Figure 6. Clearly, triple melting endotherms are observed in thermograms collected at low cooling rates (i.e. $\leq$ 20°C·min^{-1}), while double melting endotherms are observed at high cooling rates (i.e. > 20°C·min^{-1}). Triple melting endotherms were also found in the subsequent melting thermograms of PTT samples isothermally melt-crystallized at temperatures below 194°C [38]. These endotherms were labeled as peaks I, II, and III for low-, middle-, and high-temperature melting endotherm, respectively [38]. Peak I was found to correspond to the melting of the primary crystallites formed at a crystallization temperature and peaks II and III corresponded to the melting of recrystallized crystallites of different stabilities which were formed during a heating scan [38]. Qualitatively, the position of peak I shifts to a lower value with increasing cooling rate, while those of peaks II and III do not seem to be affected by changes in the cooling rate. From the relative intensities of these peaks, it can be postulated that the primary crystallites formed during non-isothermal melt-crystallization are not stable and, upon subsequent heating, these primary crystallites melt and recrystallize during further heating.

4.2. Non-isothermal melt-crystallization kinetics

4.2.1. Avrami analysis

Data analysis based on the Avrami macrokinetic equation is carried out by directly fitting the experimental $\theta(t)$ functions shown as various geometrical points in Figure 3 to Equation (3) (shown in Figure 3 as solid lines). The Avrami kinetic parameters (i.e. K_A and n_A) along with the r^2 parameters, indicating the goodness of the data fitting, were obtained from the best fits. These parameters are summarized in Table 4. The Avrami exponent n_A is found to range from ca. 4.4 to 4.7, with the average value being ca. 4.6 and the standard deviation being ca. 0.1. The Avrami crystallization rate constant K_A is found to increase with increasing cooling rate, suggesting an increased crystallization rate with increasing cooling rate.

4.2.2. Tobin analysis

Data analysis based on the Tobin macrokinetic equation is carried out by directly fitting the experimental $\theta(t)$ functions shown as various geometrical points in Figure 3 to Equation (4) (shown in Figure 3 as dotted lines). The Tobin kinetic parameters (i.e. K_T and n_T) along with the r^2 parameters, indicating the goodness of the data fitting, were obtained from the best fits. These parameters are summarized in Table 4. The Tobin exponent n_T is found to range from ca. 6.8 to 7.3, with the average value being ca. 7.0 and the standard deviation being ca. 0.2. The Tobin crystallization rate constant K_T is found to increase with increasing cooling rate, suggesting an increased crystallization rate with increasing cooling rate.

4.2.3. Comparison between results obtained from Avrami and Tobin analyzes

A direct comparison between the results obtained form the two models suggests that both of the Avrami and the Tobin crystallization rate constants (i.e. K_A and K_T, respectively) are quite comparable, with the K_A value being the smaller of the two for a given cooling rate. The results also shows that, for a given cooling rate, the Avrami exponent n_A is always lower in value than that of the Tobin one n_T. The difference between the values of n_T and n_A is ca. 2.5, with the standard deviation being ca. 0.1. The best way to test the efficiency of both models in describing the non-isothermal melt-crystallization kinetics of PTT is to reconstruct the $\theta(t)$ functions from the results summarized in Table 4 according to Equations (3) and (4) for the Avrami and the Tobin models, respectively. The reconstructed $\theta(t)$ curves according to the Avrami and the Tobin models are shown in Figure 3 as solid and dotted lines, respectively. Qualitatively, it is obvious that the Avrami model provides a much better prediction of the experimental data than does the Tobin model.

4.2.4. Ozawa analysis

By simply replacing t in Equation (1) with T/ϕ, Ozawa [24] was able to extend the Avrami model to describe the kinetics of non-isothermal crystallization.

In this approach, the raw data is the relative crystallinity function of temperature $\theta(T)$ such as those shown in Figure 2. Data analysis according to this model can be accomplished by performing a double logarithmic plot of $\ln[-\ln(1-\theta(T))]$ versus $\ln(\phi)$ for a fixed temperature, where n_O is taken as the negative value of the slope and K_O is taken as the antilogarithmic value of the ratio of the y-intercept and n_O [i.e. $K_O = \exp(y-\text{intercept}/n_O)$]. Figure 7 shows typical Ozawa plots from the raw data shown in Figure 2 for PTT within the temperature range of 160 to 186°C, while Table 5 summarizes the Ozawa kinetic parameters (i.e. K_O and n_O), including the r^2 parameter. Qualitatively, the Ozawa model was satisfactory in describing the non-isothermal melt-crystallization data of PTT. The Ozawa exponent n_O is found, in general, to increase from ca. 2.4 to ca. 4.4 with increasing temperature. The increase in the n_O value with increasing temperature is expected when the temperature range of interest is in the nucleation-controlled region. This is because the number of the athermal nuclei is found to increase tremendously with decreasing temperature [39,40], causing the nucleation mechanism to be more instantaneous in time which decreases the values of n_O. The Ozawa crystallization rate constant K_O is found to decrease with increasing temperature as normally would for crystallization in the nucleation-controlled region, suggesting a slower cooling rate at higher temperature.

4.2.5. Ziabicki's kinetic crystallizability analysis

Analysis according to the modified first order Ziabicki's kinetic equation (i.e. Equation 9) can be carried out by differentiating the relative crystallinity function of temperature $\theta(T)$, such as those shown in Figure 2, with respect to temperature in order to obtain the derivative relative crystallinity as a function of temperature $(d\theta/dT)_\phi$. Once the $(d\theta/dT)_\phi$ function is obtained, various kinetic parameters (i.e. the maximum crystallization rate $(d\theta/dT)_{\phi,max}$ and the width at half-height of the $(d\theta/dT)_\phi$ function D_ϕ) can then be obtained and the cooling rate-dependent kinetic crystallizability $G_{Z,\phi}$ can be calculated according to Equation (9). Table 6 summarizes values of $T_{max,\phi}$ (i.e. the temperature at the maximum crystallization rate as determined from the $(d\theta/dT)_\phi$ function), $(d\theta/dT)_{\phi,max}$, D_ϕ, $G_{Z,\phi}$, and, finally, G_Z. It should be noted that the values of $T_{max,\phi}$ listed in Table 6 and T_p

(i.e. the temperature at the maximum crystallization rate as determined from the raw non-isothermal melt-crystallization exotherms) listed in Table 1 are practically identical. According to Table 6, the $T_{max,\phi}$ value is found to decrease, while the $(d\theta/dT)_{\phi,max}$, D_ϕ, and $G_{Z,\phi}$ are all found to increase, with increasing cooling rate. After normalizing $G_{Z,\phi}$ value with the cooling rate, the value of the kinetic crystallizability at unit cooling rate G_Z can be determined and the results summarized in Table 6 confirm that the normalized G_Z values obtained for different cooling rates were almost identical, with the average value being 0.98.

4.2.6. Effective energy barrier for non-isothermal melt-crystallization process

Analysis based on the differential iso-conversional method of Friedman starts with the conversion of a $\theta(T)$ function, such as those shown in Figure 2, into a $\theta(t)$ function, such as those shown in Figure 3. The converted $\theta(t)$ function is then differentiated with respect to time to obtain the instantaneous crystallization rate function of time $\dot{\theta}_\theta(t)$. A plot according to Equation (10) can then be performed for various values of relative crystallinity θ using the data obtained from the $\dot{\theta}_\theta(t)$ and the $\theta(T)$ functions and, finally, the effective energy barrier for non-isothermal melt-crystallization process for a given θ (i.e. ΔE_θ) can be determined, as a result, from the slope of the plot [i.e. ΔE_θ = -(slope)(R)]. The ΔE_θ values determined for various values of θ, ranging from 0.1 to 0.9 with 0.1 increment, are summarized in Table 7. Apparently, the ΔE_θ parameter is found to increase monotonically from -129.4 $kJ \cdot mol^{-1}$ at $\theta = 0.1$ to -83.3 $kJ \cdot mol^{-1}$ at $\theta = 0.9$, suggesting that, as the crystallization progressed, it was more difficult for the polymer to crystallize.

5. CONCLUSIONS

The non-isothermal melt-crystallization kinetic and the subsequent melting behavior of PTT for eight different cooling rates were investigated. The non-isothermal melt-crystallization exotherms of PTT showed that the temperature at 1% relative crystallinity, the temperature at the maximum crystallization rate, and the temperature at 99% relative crystallinity were all shifted towards lower temperatures

with an increase in the cooling rate investigated, indicating that PTT took a shorter time to crystallize as cooling rate increased. Further analysis of the non-isothermal melt-crystallization behavior revealed that the apparent incubation period, the crystallization time at different relative crystallinity values, and the apparent total crystallization period were all found to decrease with increasing cooling rate. Interestingly, both the crystallization time at different relative crystallinity values and the apparent total crystallization period showed a linear relationship with the cooling rate in the log-log plots, with all the plots exhibiting a regression line of similar slope (i.e. the average value being ca. –0.725 $min^{2}\cdot{}^{o}C^{-1}$). The subsequent melting behavior of PTT (recorded with a heating rate $10^{o}C\ min^{-1}$) after non-isothermal melt-crystallization in DSC at eight different cooling rates showed that the melting of PTT exhibited triple melting endotherms when it was crystallized at low cooling rates (i.e. $\leq 20^{o}C\cdot min^{-1}$), while it showed double melting endotherms when it was crystallized at high cooling rates (i.e. $> 20^{o}C\cdot min^{-1}$).

The Avrami and the Tobin models were all found to describe the non-isothermal melt-crystallization data of PTT fairly well, with the Avrami model being the better of the two. The average values of the Avrami and the Tobin exponents are ca. 4.6 and 7.0, respectively. Both the Avrami and Tobin crystallization rate constants were found to increase with increasing cooling rate. The Ozawa model was also found to describe the non-isothermal melt-crystallization data of PTT fairly well. The Ozawa exponent was found to be a slight increasing function, while the Ozawa crystallization rate constant was found to be a decreasing function, with the temperature. The ability for PTT to crystallize from the molten state under a unit cooling rate was evaluated based on the Ziabicki's kinetic crystallizability, from which it was found to be 0.98. Lastly, the effective energy barrier governing the non-isothermal melt-crystallization of PTT was found to increase monotonically with increasing relative crystallinity value.

ACKNOWLEDGEMENTS

The authors wish to thank Dr. Hoe Chuah and his colleagues of Shell Chemical Company (USE) Ltd. for supplying PTT resin and for their kind assistance

with molecular weight measurements. Partial supports for this work from the Petroleum and Petrochemical Technology Consortium (through a governmental loan from the Asian Development Bank) and the Petroleum and Petrochemical College are gratefully acknowledged.

REFERENCES

[1] Whinfield JR and Dickson JT, *Brit Pat* (14 June 1946).

[2] Process Economics Program Report: 227. 1,3-Propanediol and Poly(trimethylene terephthalate), SRI International (1999).

[3] Ward IM and Wilding MA, *J Polym Sci Polym Phys* **14**:263 (1976).

[4] Jakeways R, Ward IM and Wilding MA, *J Polym Sci Polym Phys* **13**:799 (1975).

[5] Ho RM, Ke KZ and Chen M, *Macromolecules* **33**:7529 (2000).

[6] Wang B, Li CY, Hanzlicek J, Cheng SZD, Geil PH, Grebowicz J and Ho RM, *Polymer* **42**:7171 (2001).

[7] Chuah HH, *Polym Engng Sci* **41**:308 (2001).

[8] Huang JM and Chang FC, *J Polym Sci Polym Phys* **38**:934 (2000).

[9] Hong PD, Chung WT and Hsu CF, *Polymer* **43**:3335 (2002).

[10] Wang XS, Yan D, Tian GH and Li XG, *Polym Engng Sci* **41**:1655 (2001).

[11] Dangseeyun N, Srimoaon P, Supaphol P and Nithitanakul M, *Thermochim Acta* **409**:63 (2004).

[12] Chen M, Chen CC, Ke KZ and Ho RM, J Macromol Sci Phys 41:1063 (2002).

[13] Supaphol P, Dangseeyun N, Srimoaon P and Nithitanakul M, *Thermochim Acta* **406**:207 (2003).

[14] Supaphol P, Dangseeyun N and Srimoaon P, *Polym Test* **23**:175 (2004).

[15] Avrami M, *J Chem Phys* **7**:1103 (1939).

[16] Avrami M, *J Chem Phys* **8**:212 (1940).

[17] Avrami M, *J Chem Phys* **9**:177 (1941).

[18] Wunderlich B, *Macromolecular Physics*, Vol. 2, Academic Press, New York, pp 147 (1976).

[19] Supaphol P, *J Appl Polym Sci* **78**:338 (2000).

[20] Zhang QX, Zhang ZH, Zhang HF and Mo ZS, *J Polym Sci Polym Phys* **40**:1784 (2002).

[21] Tobin MC, *J Polym Sci Polym Phys* **12**:399 (1974).

[22] Tobin MC, *J Polym Sci Polym Phys* **14**:2253 (1976).

[23] Tobin MC, *J Polym Sci Polym Phys* **15**:2269 (1977).

[24] Evans UR, *Trans Faraday Soc* **41**:365 (1945).

[25] Ozawa T, *Polymer* **12**:150 (1971).

[26] Ziabicki A, *Appl Polym Symp* **6**:1 (1967).

[27] Ziabicki A, *Polymery* **12**:405 (1967).

[28] Ziabicki A, *Fundamentals of Fiber Spinning*, John Wiley & Sons, New York, pp 112–114 (1976).

[29] Jeziorny A, *Polymer* **19**:1142 (1978).

[30] Augis JA and Bennett JE, *J Therm Anal* **13**:283 (1978).

[31] Kissinger HE, *J Res Natl Bur Stand* **57**:217 (1956).

[32] Takhor RL, *Advances in Nucleation and Crystallization of Glasses*, American Ceramics Society, Columbus, pp. 166-172 (1971).

[33] Vyazovkin S, *Macromol Rapid Commun* **23**:771 (2002).

[34] Friedman H, *J Polym Sci* **C6**:183 (1964-1965).

[35] Vyazovkin S, *J Comput Chem* **18**:393 (1997).

[36] Vyazovkin S, *J Comput Chem* **22**:178 (2001).

[37] Supaphol P, Srimoaon P and Sirivat A, *Polym Int*, in press.

[38] Srimoaon P, Dangseeyun N and Supaphol P, *Eur Polym J*, in press.

[39] Supaphol P and Spruiell JE, *J Appl Polym Sci* **75**:337 (2000).

[40] Janeschitz-Kriegl H, Ratajski E and Wippel H, *Colloid Polym Sci* **277**:217 (1999).

CAPTIONS OF FIGURES

Figure 1. Non-isothermal melt-crystallization exotherm of PTT at eight different cooling rates.

Figure 2. Relative crystallinity function of temperature of PTT at eight different cooling rates. The data have been converted from the data shown in Figure 1 using Equation (1).

Figure 3. Relative crystallinity function of time of PTT for eight different cooling rates. The data have been converted from the data shown in Figure 2 using Equation (2). Different geometrical points represent the raw data, while the solid and the dotted lines are the Avrami and the Tobin predictions, respectively.

Figure 4. Crystallization time at various relative crystallinity values as a function of cooling rate. The inset figure shows relationship between apparent total crystallization period and cooling rate in a log-log plot.

Figure 5. Relationship between crystallization time at various relative crystallinity values and cooling rate in a log-log plot.

Figure 6. Subsequent melting endotherm of PTT (recorded at $10^{o}C \cdot min^{-1}$) after non-isothermal melt-crystallization at eight different cooling rates.

Figure 7. Typical Ozawa analysis based on the non-isothermal melt-crystallization data of PTT.

Table 1. Characteristic data of non-isothermal melt-crystallization exotherms for PTT.

ϕ (°C·min^{-1})	$T_{0.01}$ (°C)	T_p (°C)	$T_{0.99}$ (°C)
5.0	191.6	183.0	176.9
7.5	184.6	179.6	173.4
10.0	186.2	176.6	169.9
12.5	185.5	174.8	166.6
15.0	183.2	172.3	162.4
20.0	180.2	168.7	159.4
25.0	177.6	164.7	154.8
30.0	176.3	163.5	153.2

Table 2. Quantitative analysis of the relative crystallinity functions of time which were converted from non-isothermal melt-crystallization of PTT.

ϕ	Δt_{inc}	t_θ (min)							Δt_c
($^oC \cdot min^{-1}$)	(min)	θ = 0.01	θ = 0.1	θ = 0.3	θ = 0.5	θ = 0.7	θ = 0.9	θ = 0.99	(min)
5.0	15.81	0.87	1.64	2.16	2.48	2.78	3.19	3.81	2.94
7.5	10.91	0.59	1.14	1.51	1.75	1.96	2.25	2.63	2.04
10.0	8.40	0.48	0.91	1.20	1.39	1.56	1.79	2.12	1.64
12.5	6.78	0.37	0.77	1.03	1.20	1.35	1.56	1.89	1.52
15.0	5.73	0.39	0.73	0.95	1.09	1.23	1.43	1.78	1.39
20.0	4.45	0.29	0.55	0.72	0.84	0.95	1.11	1.32	1.04
25.0	3.62	0.27	0.50	0.66	0.77	0.87	1.00	1.19	0.91
30.0	3.06	0.23	0.42	0.55	0.64	0.72	0.84	1.00	0.77

Remark: Δt_{inc} is calculated based on a fixed fusion temperature of 275°C.

Table 3. Y-intercept, slope, and the r^2 values of regression lines drawn through plots of $\ln(t_\theta)$ against $\ln(\phi)$ for various relative crystallinity values.

θ	Y-intercept (min)	slope ($min^2\ ^oC^{-1}$)	r^2
0.01	0.94	-0.715	0.978
0.1	1.63	-0.736	0.993
0.3	1.92	-0.737	0.995
0.5	2.05	-0.733	0.995
0.7	2.16	-0.728	0.995
0.9	2.28	-0.721	0.995
0.99	2.45	-0.716	0.991
	Average	-0.727	

Table 4. Non-isothermal melt-crystallization kinetics for PTT based on Avrami and Tobin analyses.

		Avrami analysis			Tobin analysis		
ϕ (°C min^{-1})	$t_{0.5}^{-1}$ (min^{-1})	n_A	K_A (min^{-1})	r^2	n_T	K_T (min^{-1})	r^2
5.0	0.40	4.69	0.373	1.000	7.29	0.410	0.998
7.5	0.57	4.67	0.531	1.000	7.09	0.583	0.997
10.0	0.72	4.63	0.668	1.000	7.10	0.736	0.997
12.5	0.83	4.47	0.770	1.000	7.03	0.850	0.997
15.0	0.92	4.61	0.844	1.000	7.10	0.930	0.997
20.0	1.19	4.39	1.095	1.000	6.77	1.210	0.998
25.0	1.30	4.51	1.202	1.000	6.83	1.326	0.997
30.0	1.56	4.47	1.440	1.000	6.84	1.594	0.997

Table 5. Non-isothermal melt-crystallization kinetics for PTT based on Ozawa analysis.

Temperature (°C)	n_O	K_O (°C·min^{-1})	r^2
160	2.40	35.631	0.956
162	2.67	30.007	0.955
164	2.64	25.625	0.978
166	2.99	21.937	0.984
168	3.26	18.941	0.993
170	3.56	16.478	0.994
172	3.66	14.026	0.994
174	3.70	11.703	0.991
176	3.99	10.039	0.991
178	3.45	7.918	0.980
180	3.42	6.564	0.990
182	3.68	5.405	0.989
184	3.64	4.284	0.992
186	4.37	3.680	0.992

Table 6. Non-isothermal melt-crystallization kinetics for PTT based on Ziabicki's kinetic crystallizability analysis.

ϕ ($^{o}C \cdot min^{-1}$)	$T_{max,\phi}$ (^{o}C)	$(d\theta/dT)_{\phi,max}$ (min^{-1})	D_{ϕ} (^{o}C)	$G_{Z,\phi}$ ($^{o}C\ min^{-1}$)	G_Z
5.0	183.0	0.68	6.73	4.86	0.97
7.5	179.6	0.95	7.29	7.36	0.98
10.0	176.6	1.18	7.84	9.85	0.98
12.5	174.8	1.33	8.65	12.21	0.98
15.0	172.3	1.50	9.09	14.53	0.97
20.0	168.7	1.85	10.01	19.66	0.98
25.0	164.7	2.05	11.37	24.79	0.99
30.0	163.5	2.43	11.52	29.73	0.99
				Average	0.98

Table 7. Effective energy barrier describing the overall non-isothermal melt-crystallization of PTT based on the differential iso-conversional method of Friedman.

θ	ΔE_θ (kJ·mol^{-1})	r^2
0.1	-129.4	0.983
0.2	-118.3	0.979
0.3	-110.5	0.976
0.4	-104.4	0.974
0.5	-99.2	0.972
0.6	-94.6	0.970
0.7	-90.4	0.968
0.8	-86.3	0.964
0.9	-83.3	0.952

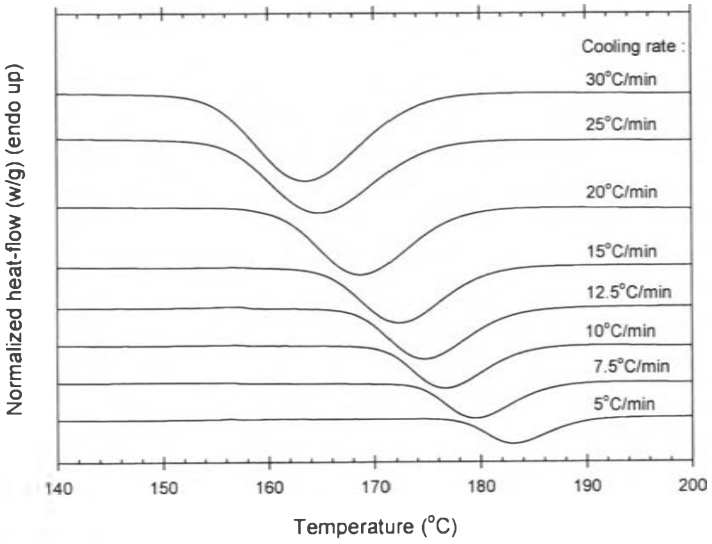
Cooling rate :
30°C/min
25°C/min
20°C/min
15°C/min
12.5°C/min
10°C/min
7.5°C/min
5°C/min
Normalized heat-flow (w/g) (endo up)
140
150
160
170
180
190
200
Temperature (°C)

Figure 1

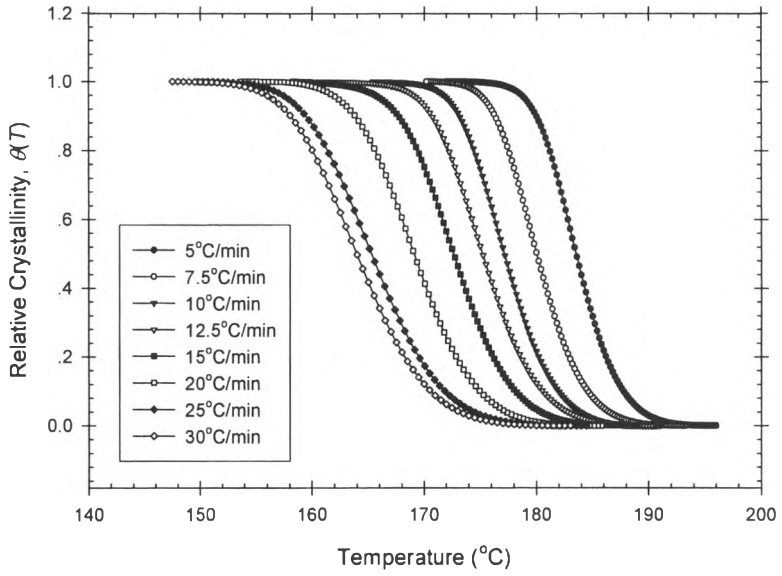
1.2
1.0
.8
.6
.4
.2
0.0
Relative Crystallinity, θ(T)
140
150
160
170
180
190
200
Temperature (°C)
5°C/min
7.5°C/min
10°C/min
12.5°C/min
15°C/min
20°C/min
25°C/min
30°C/min

Figure 2

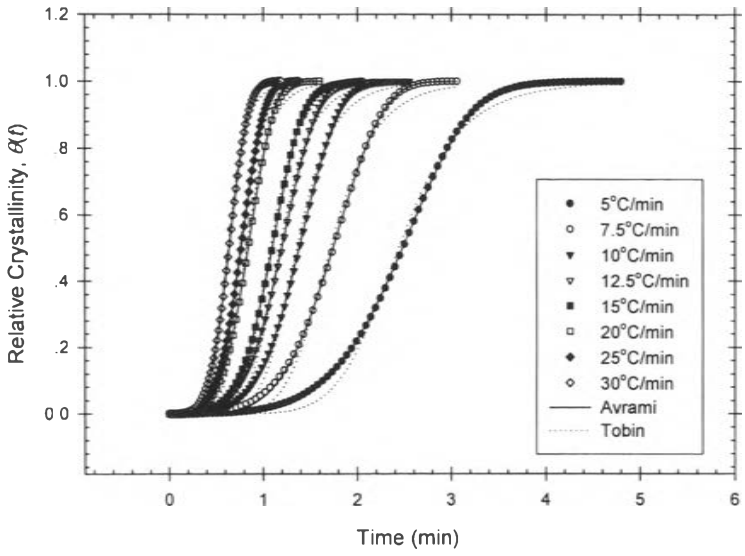
Relative Crystallinity, θ(t)
1.2
1.0
.8
.6
.4
.2
0 0
0
1
2
3
4
5
6
Time (min)
5°C/min
7.5°C/min
10°C/min
12.5°C/min
15°C/min
20°C/min
25°C/min
30°C/min
Avrami
Tobin

Figure 3

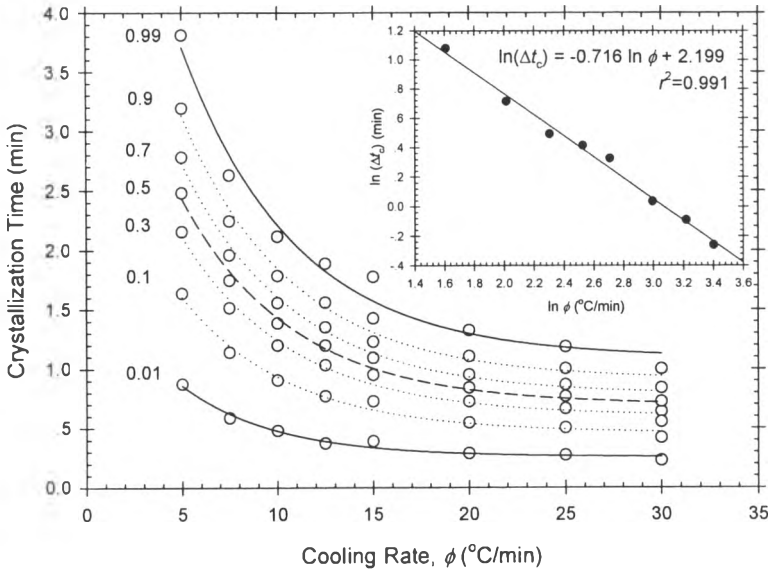
Crystallization Time (min)
Cooling Rate, ϕ (°C/min)
0.99
0.9
0.7
0.5
0.3
0.1
0.01
$\ln(\Delta t_c) = -0.716 \ln \phi + 2.199$
r^2=0.991
ln (Δt_c) (min)
ln ϕ (°C/min)

Figure 4

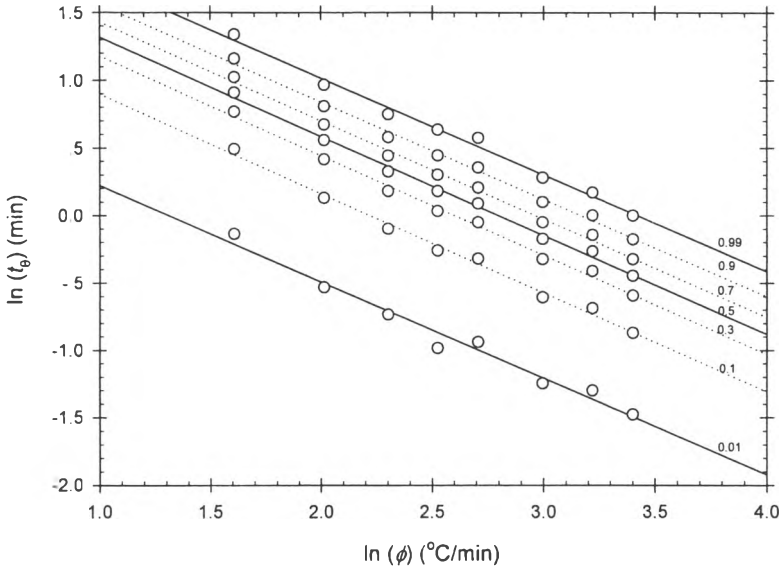
1.5
1.0
5
0.0
-5
-1.0
-1.5
-2.0
1.0
1.5
2.0
2.5
3.0
3.5
4.0
ln (t_θ) (min)
ln (ϕ) (°C/min)
0.99
0.9
0.7
0.5
0.3
0.1
0.01

Figure 5

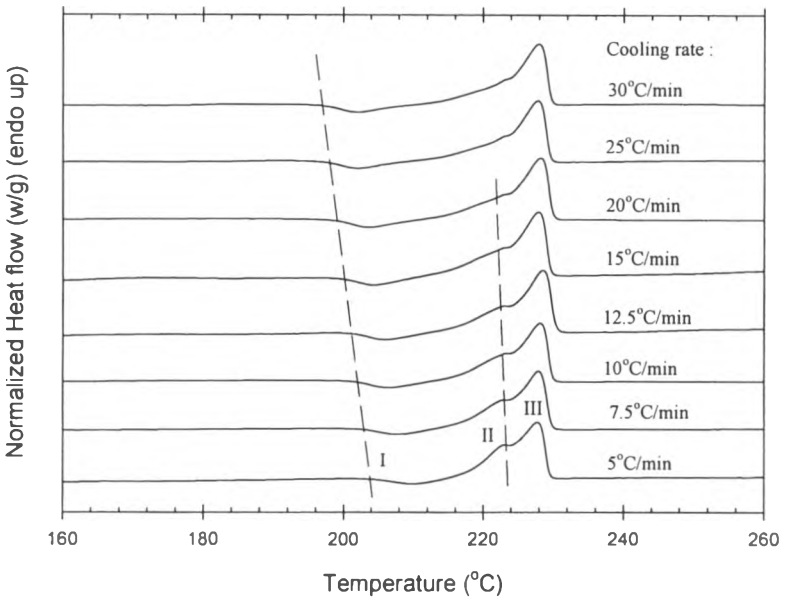
Cooling rate :
30°C/min
25°C/min
20°C/min
15°C/min
12.5°C/min
10°C/min
7.5°C/min
5°C/min
I
II
III
Normalized Heat flow (w/g) (endo up)
160
180
200
220
240
260
Temperature (°C)

Figure 6

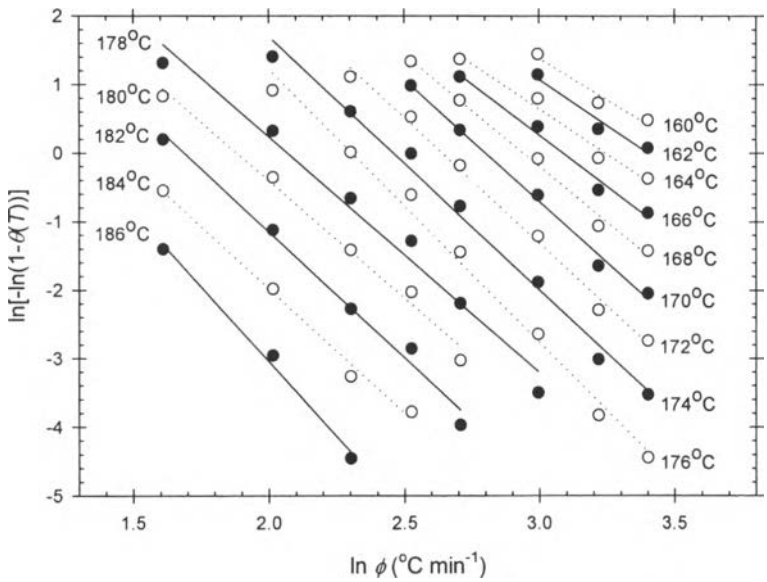
178°C
180°C
182°C
184°C
186°C
160°C
162°C
164°C
166°C
168°C
170°C
172°C
174°C
176°C
ln[-ln(1-α(T))]
ln φ (°C min-1)
2
1
0
-1
-2
-3
-4
-5
1.5
2.0
2.5
3.0
3.5

Figure 7